Passive Wireless Vibration Sensing for Measuring Aerospace Structural Flutter

William C. Wilson, Jason P. Moore
Nondestructive Evaluation Sciences Branch
NASA Langley Research Center
Hampton, VA, USA
William.C.Wilson@nasa.gov

***Abstract*— To reduce energy consumption, emissions, and noise, NASA is exploring the use of high aspect ratio wings on subsonic aircraft. Because high aspect ratio wings are susceptible to flutter events, NASA is also investigating methods of flutter detection and suppression. In support of that work a new remote, non-contact method for measuring flutter-induced vibrations has been developed. The new sensing scheme utilizes a microwave reflectometer to monitor the reflected response from an aeroelastic structure to ultimately characterize structural vibrations. To demonstrate the ability of microwaves to detect flutter vibrations, a carbon fiber–reinforced polymer (CFRP) composite panel was vibrated at various frequencies from 1Hz to 130Hz. The reflectometer response was found to closely resemble the sinusoidal response as measured with an accelerometer up to 100 Hz. The data presented demonstrate that microwaves can be used to measure flutter-induced aircraft vibrations.**

Keywords- SHM, IVHM, RF, Microwave, Fluttter, Sensors

I. INTRODUCTION

NASA is investigating structural flutter effects in aeroelastic wings through multiple projects within its Advanced Air Vehicles Program (AAVP) and the Advanced Air Transport Technology (AATT) Project. One collaborative project with Boeing is called the Subsonic Ultra-Green Aircraft Research (SUGAR), and is examining the aeroelasticity of high aspect ratio wings such as the truss-braced wing design for commercial aircraft (Fig. 1). The goal is to reduce energy consumption, emissions, and noise [1]. In another collaborative project, NASA and the Royal Institute of Technology (KTH) are investigating the behavior of flexible wings on military aircraft. The primary concern is nonlinear aeroelastic limit cycle oscillations (flutter) [2]. NASA is also investigating whirl induced flutter on light-weight flexible aircraft structures using the X-57 Maxwell all-electric multi-engine aircraft [3].

New aircraft like the Boeing 787 and Bombardier's C Series are increasing the aspect ratio of in-production wings to ~9 and are additionally allowing increased aeroelastic flexibility in wings to minimize weight. The desire to push aspect ratios even higher is increasing the need for reliable flutter suppression schemes [4]. While flexible high aspect ratio wings may lead to more efficient aircraft, they may also lead to increased flutter conditions and onset of flutter at lower speeds of operation [5].

Sponsored by NASA's Advanced Air Transport Technology (AATT) Project

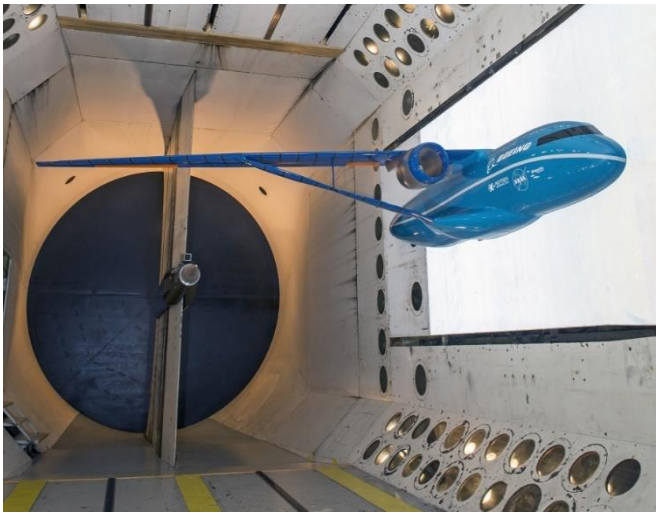

Figure 1. Truss Braced Wing (TBW) in NASA's Transonic Dynamics Tunnel (TDT).

In response to the increasing need for flutter detection mechanisms, methods traditionally associated with structural health monitoring (SHM) are being re-investigated for possible applicability in highly-flexible aerospace applications [6]. Strain gauges [7, 8] and accelerometers [9, 10] have been used to measure flutter, along with piezoelectric sensors [11, 12], microelectromechanical systems (MEMS) [13], and fiber optic strain sensors [14-16] in vibration and load monitoring applications. Surface acoustic wave (SAW) devices have been investigated for flutter applications because they are small, lightweight, low power, and can be deployed wired or wirelessly [17]. Similarly microwave techniques can operate as a fully passive wireless flutter sensing system without any sensors bonded to the structure. Microwave displacement systems have been used for measuring movement in bridges [18] and stay cables [19].

In support of NASA's programs investigating high aspect ratio wings, a new microwave-based method for measuring flutter-induced vibrations has been developed. The new sensing scheme utilizes a network analyzer connected to a horn antenna to form a microwave reflectometer which records the reflection response of a structure in order to detect vibrations.

II. Experimental Setup

The test setup consists of a network analyzer, a horn antenna, a composite test panel, and a shaker (Fig. 2). The carbon fiber–reinforced polymer (CFRP) composite panel measuring 406 mm by 406 mm by 2.78 mm was fabricated at NASA Langley Research Center. The composite panel is quasi-isotropic, made up of Hexcel® IM7/8552 (IM7 fibers and 8552 prepreg resin) with a 26 ply thick layup of $[(0/+45/-45/90)_3\ 0]_S$. Details of the material properties are available in a prior paper by Leckey et al [20].

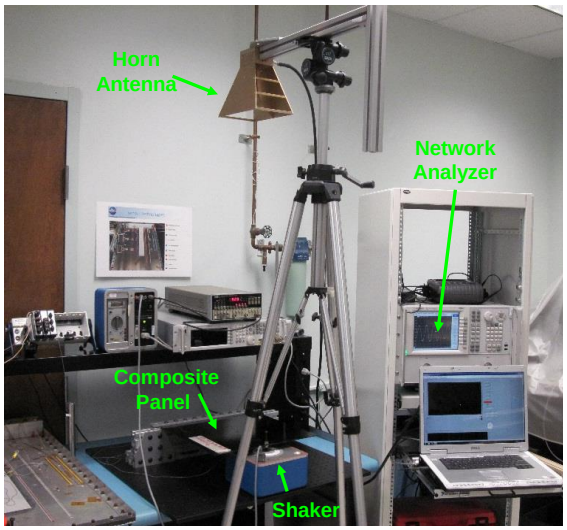

Figure 2. The test setup showing the network analyzer, the horn antenna, the composite test panel, and the shaker.

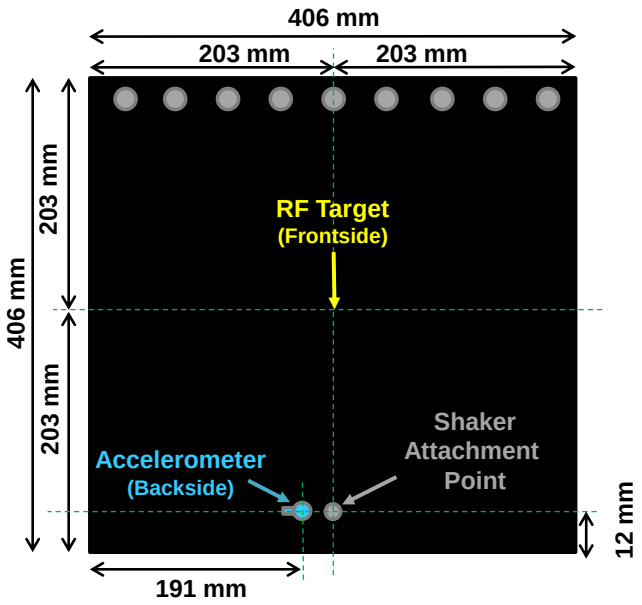

Figure 3. A diagram showing the location and distances of the accelerometer (underside), the RF target area and the shaker attachment location.

A Dytran Instruments, Inc. Miniature Accelerometer, model number 3035B1G, was bonded to backside of the panel at the location shown in Fig. 3. An HP 8116A function generator drives an APS Dynamics model 300-C Portable Shaker-Amplifier attached to the free end of the cantilevered panel to simulate flutter by inducing structural vibration. The horn antenna is connected to an Agilent Technologies 6 GHz Network Analyzer, model N5230C, while the accelerometer signal is sampled using the National Instruments™ cDaq-9178 data acquisition system with a NI 9232 input module.

The center frequency of the swept-frequency interrogation signal is 1994.7 MHz, giving a center wavelength of 150.4 mm. The antenna's largest dimension is 244 mm. Eq. 1 shows that the minimum distance for far field operation is 792 mm, where d_f is the far field distance (792 mm), D is the largest antenna aperture dimension (244 mm), and λ is the wavelength (150.4 mm).

$$d_f = 2\left(D^2\right)/(\lambda) \tag{1}$$

Because the antenna-to-panel distance is set to 1 m, the measurements are accordingly made in the far field.

The complex scattering parameter S_{11} (the reflection coefficient) is recorded for a narrow band of frequencies (1994.65 MHz to 1994.75 MHz) using the network analyzer. Because the vibration of the panel dynamically affects the distance between the antenna and the reflective panel, the vibration effect appears in the phase of the S_{11} response. As an example, Fig. 4 shows the S_{11} phase response for an induced 2 Hz vibration in the panel. The unfiltered phase response (blue line) is plotted along with the low-pass filtered phase response (red dashed line). The downward trend in the filtered phase response is a result of the sweeping microwave frequency during S_{11} acquisition. Environmental effects are considered insignificant in this investigation, as they are assumed to be near steady state (frequencies below 1 Hz).

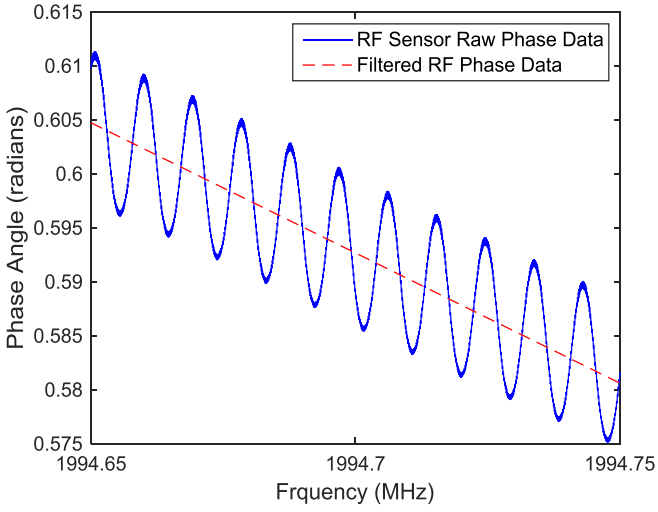

Figure 4. The microwave raw phase data measuring a 2 Hz sine wave.

Subtracting the filtered phase response from the unfiltered phase response yields the dynamic phase data shown in Fig. 5.

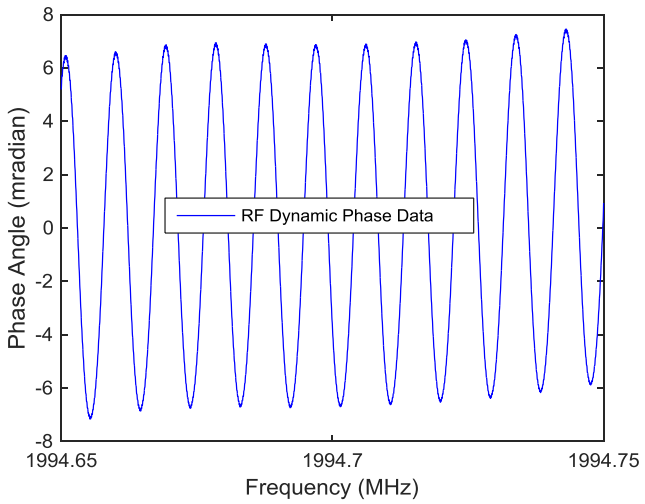

Figure 5. The S_{11} dynamic phase data resulting from subtraction of filtered phase data (Fig. 4 in red) from the unfiltered phase data (Fig. 4 in blue).

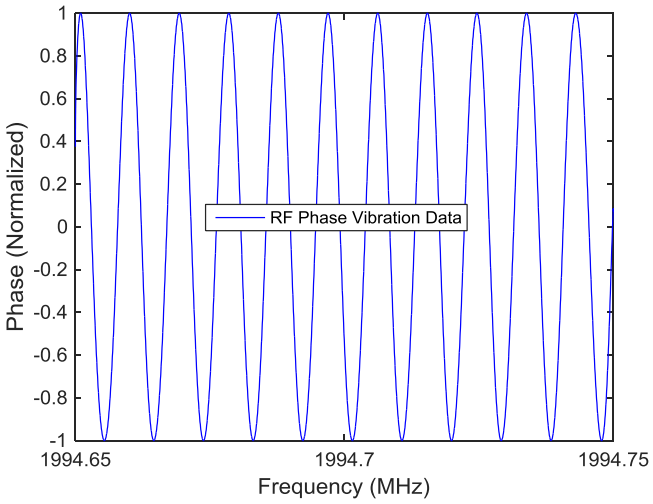

Figure 7. The microwave vibration data, calculated by dividing the dynamic phase data of Fig. 5 by the analytic signal of the dynamic phase data of Fig. 6.

The dynamic phase data clearly shows a vibrational component which matches the frequency of the panel vibration. Because the accelerometer was not located at the area of microwave interrogation, only the vibrational *frequency* response is analyzed at this time. In order to compare the vibrational frequency measurements of the S_{11} phase response and the accelerometer data, the amplitude of the dynamic phase response is normalized across the microwave frequency band using the Hilbert transform. The Hilbert transform is calculated by using the principal value of the integral:

$$H[g(t)] = \frac{1}{\pi} \int_{-\infty}^{\infty} \frac{g(\tau)}{t-\tau} d\tau \,. \qquad (2)$$

The absolute value of the Hilbert transform of the dynamic phase data is given in Fig. 6.

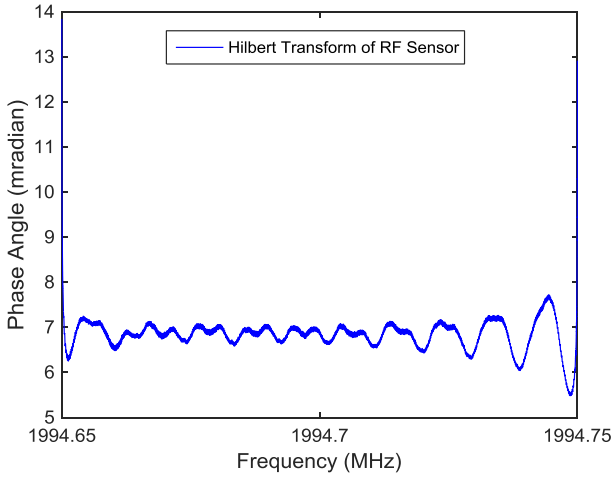

Figure 6. Hilbert transform of the dynamic phase data.

The vibration data shown in Fig. 7 is calculated by dividing the dynamic phase data (Fig. 5) by the analytic signal, or the absolute value of the Hilbert transform, of the dynamic phase data (Fig. 6). This envelope normalization yields a measurement that has a consistent amplitude for sinusoidal signals (Fig. 7). It should be noted that this method only works to remove the distortions from signals that are cyclic in nature (flutter response) and is inappropriate for processing arbitrary broadband signals.

III. Results

To demonstrate the ability of microwaves to detect flutter-like vibrations the phase data was sampled and processed for at the vibrational frequencies of 1 Hz, 2 Hz, 5 Hz, 10 Hz, 25 Hz, 50 Hz, 100 Hz, 110 Hz, 120 Hz, and 130 Hz using a sinusoidal driver signal 530 $mV_{pk\text{-}pk}$ from the function generator coupled to the shaker. The microwave data of Figs. 8-12 have been envelope-normalized as previously explained and have been additionally normalized to the accelerometer data for comparison. The x-axis of Figs. 8-12 is time-based, as the sweeping of the microwave frequency by the network analyzer requires a finite, yet repeatable, amount of time. The time scales have been adjusted to limit the number of the sinusoidal cycles displayed in the figures. However, the entirety of each data set was used for all calculations. The frequency response of the microwave and accelerometer data approximately match one another up to 100Hz. Beyond those frequencies the discrepancies are no longer minor; at 110 Hz the differences between the accelerometer and the RF data are significant.

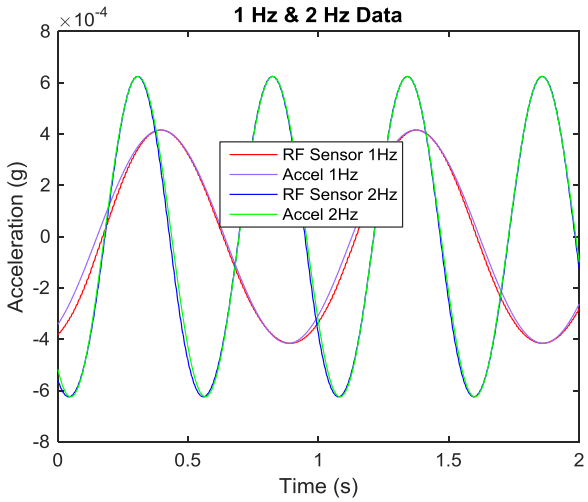

Figure 8. The microwave and accelerometer data for 1 & 2 Hz signals.

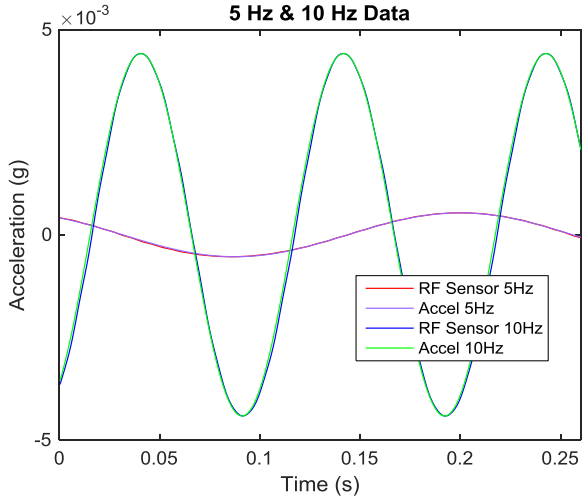

Figure 9. The microwave and accelerometer data for 5 & 10 Hz signals.

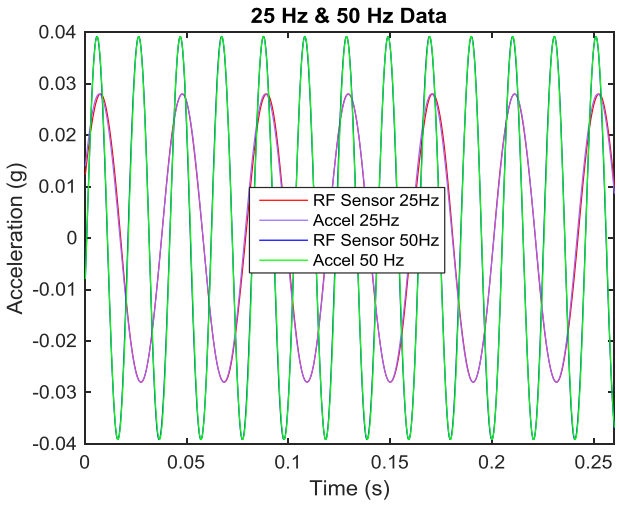

Figure 10. The microwave and accelerometer data for 25 & 50 Hz signals.

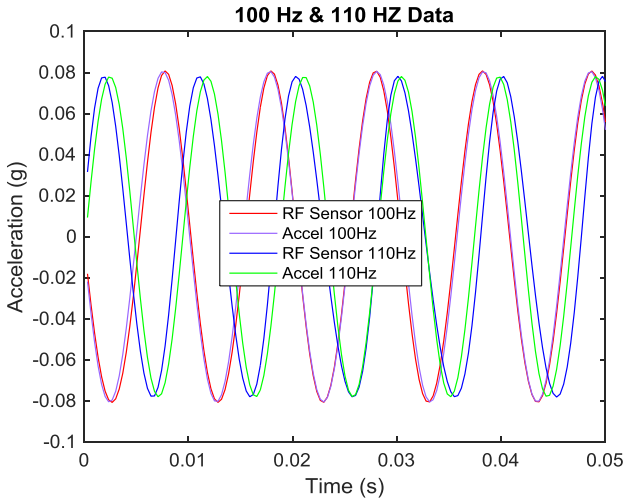

Figure 11. The microwave and accelerometer data for 100 & 110 Hz signals.

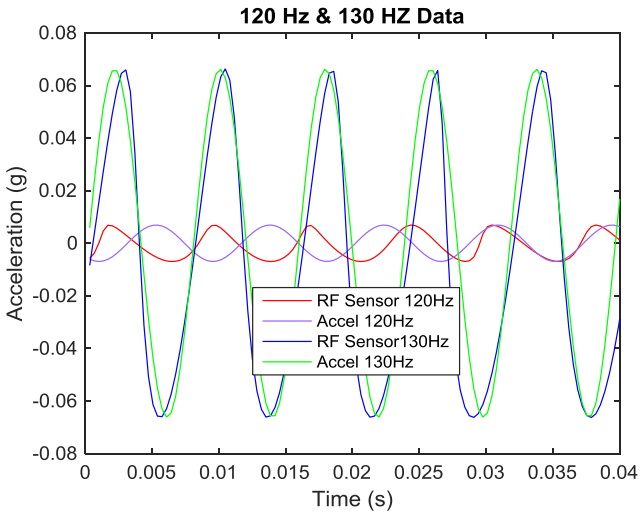

Figure 12. The microwave and accelerometer data for 120 & 130 Hz signals.

At 120 and 130 Hz there is only a sporadic match of the two sets of data, and at 120 Hz, the microwave data deviates significantly from sinusoidal behavior, possibly due to mode conversions since the amplitude is less for both the accelerometer and the RF sensor. To quantify the difference between the microwave and accelerometer data in Figures 8~12, the Pearson correlation coefficient was computed for each data set using:

$$r = \frac{\sum_{i=1}^{n}\left(x_i - \bar{x}\right)\left(y_i - \bar{y}\right)}{\sqrt{\sum_{i=1}^{n}\left(x_i - \bar{x}\right)^2}\sqrt{\sum_{i=1}^{n}\left(y_i - \bar{y}\right)^2}}. \qquad (3)$$

Where r is the correlation coefficient, n is the number of data points in each set, i is the current data point, x_i is the acceleration

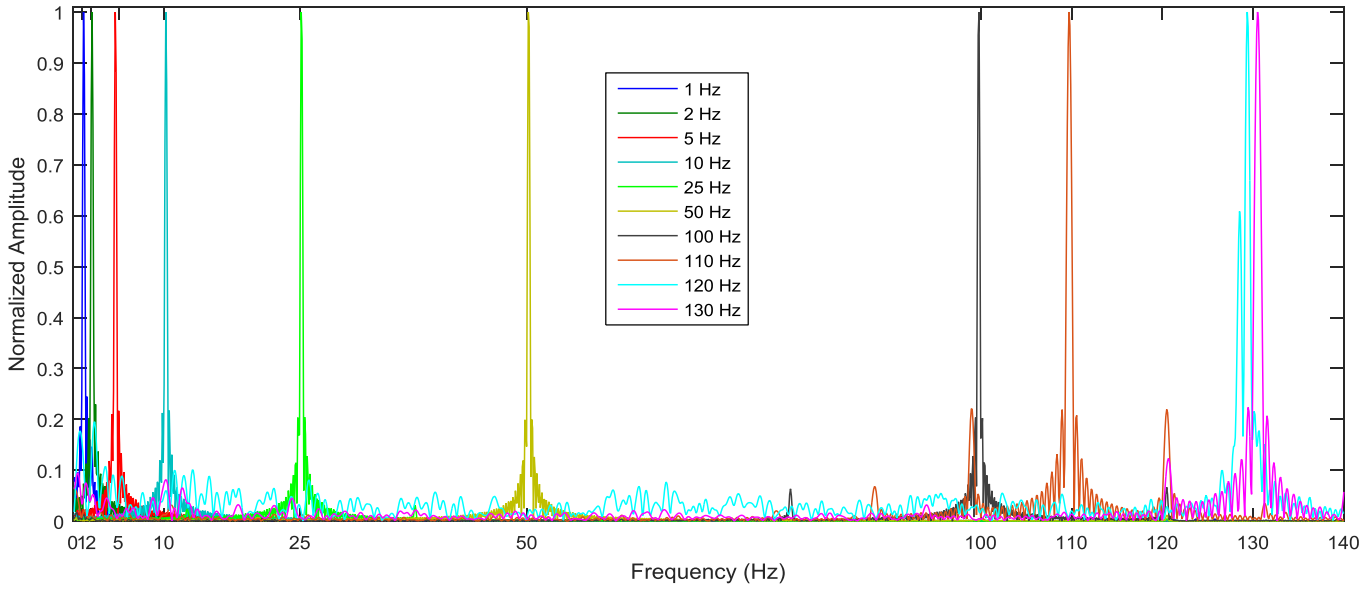

Figure 13. FFT of the microwave vibration data.

value, y_i is the microwave value, $\bar{x}$ is the mean of the acceleration values, and $\bar{y}$ is the mean of the microwave values. The correlation coefficient values are given in Table I.

The correlation of the accelerometer and microwave data is high at the lower frequencies and sharply approaches near-zero at the higher frequencies (Fig. 14), suggesting a preliminary microwave-based detection upper vibration frequency limit of 100 Hz.

Because the microwave phase-based measurement was both envelope-normalized and normalized to the accelerometer data, only the frequency response of the microwave dynamic phase measurement is analyzed here. Shown in Fig. 13 is the unity-normalized result of Fast Fourier Transforming (FFT) the microwave dynamic phase responses of Figs. 8-12.

Each of the data sets has one large peak at the fundamental frequency, however 110Hz has significant deviation that shows up as two smaller peaks at 99Hz and 121Hz. Additionally, the peaks for 120Hz and 130Hz are shifted to 129.4Hz and 130.5Hz respectively.

The most likely source of vibrational measurement error comes from the experimental setup itself. The accelerometer is mounted at the shaker-controlled end of the panel while the microwave dynamic phase data is affected by the entirety of the panel, which may be experiencing dynamic behavior other than the shaker input vibration; in particular, the higher frequency vibration input may be coupling towards a resonant vibration mode of the panel. The accelerometer may not experience the same vibration since it is directly under the area of the microwaves.

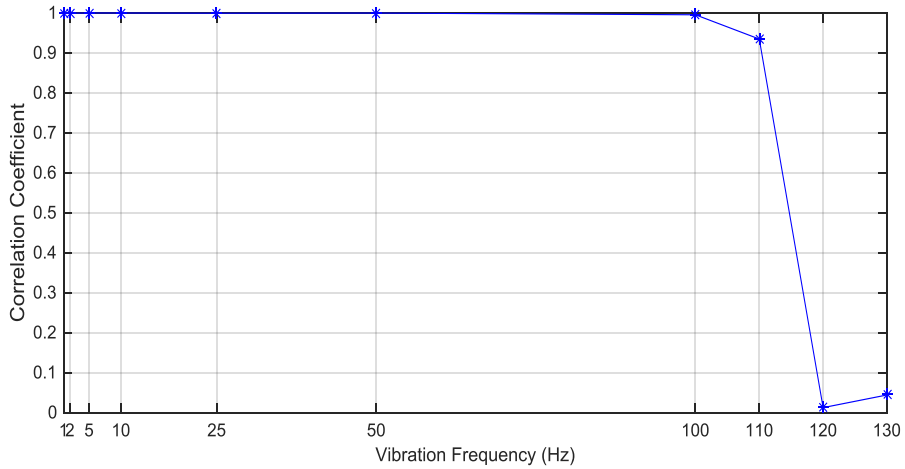

Figure 14. Correlation coefficient of the vibration data.

TABLE I. COEFFICIENT VALUES

Frequency (Hz)	Correlation Coefficient
1	9.9788e-01
2	9.9920e-01
5	9.9979e-01
10	9.9971e-01
25	9.9922e-01
50	9.9959e-01
100	9.9523e-01
110	9.3451e-01
120	1.2193e-02
130	4.3864e-02

In summary, the sinusoidal vibrations of a composite panel are accurately captured up to 100Hz and the vibrational frequency measurements are spectrally pure up to the 100Hz as well, demonstrating that microwaves can be used to detect flutter-like vibrations up to 100Hz. While the technique seemed to fail at vibration frequencies above 100Hz, there is strong possibility that the failure was in the experimental setup itself and that the technique will function well beyond 100Hz.

IV. Conclusions

A new passive, wireless, non-contact method for detection of flutter-like vibration has been presented. Relying on the reflection of microwaves from a CFRP structure, a microwave reflectometer scheme is utilized to monitor the effect of vibrations in the structure on the relative phase of the measured S_{11} response. Data has been presented that demonstrates detection of flutter-like vibrations from 1Hz to 100Hz. The microwave data is sinusoidal and closely matches the spectral response of accelerometer data. The microwaves are reflected from the structural material and therefore do not require that a sensor be attached to the structure. This technique will work on any reflective (conductive) structure. The non-contact, non-invasive nature of this flutter detection method makes it attractive for both retrofit applications and new aircraft installation.

Future work will further characterize the RF behavior to optimize the response and reduce noise. The discrepancy between the accelerometer RF data at high frequencies will be investigated. Additionally, the successful demonstration of the technique for the detection of vibrations above 100Hz may be possible through the use of an augmented experimental setup, and/or a change of parameters to allow for higher sampling rates for higher frequencies. Additionally, techniques to enable the measurement of multiple structural locations simultaneously via a single antenna, such as through the use of frequency division multiplexing FDM or frequency selective surfaces will be considered.

References

[1] R. C. Scott, R. E. Bartels, *et al.*, "Aeroservoelastic Test of the Subsonic Ultra-Green Aircraft Research Truss-Braced Wing Model," *Journal of Guidance, Control, and Dynamics*, vol. 39, no. *8*, pp. 1820-1833, Aug. 2016.

[2] W. A. Silva, P. Chwalowski, *et al.*, "Computational Results for the KTH-NASA Wind-Tunnel Model Used for Acquisition of Transonic Nonlinear Aeroelastic Data," in *Proc. 58th AIAA/ASCE/AHS/ASC Structures, Structural Dynamics, and Materials Conference*, Grapevine, TX, AIAA 2017-1814, Jan. 9-13, 2017, p. 20.

[3] C. B. Hoover, J. Shen, *et al.*, "Whirl Flutter Stability and Its Influence on the Design of the Distributed Electric Propeller Aircraft X-57," in *Proc. 17th AIAA Aviation Technology, Integration, and Operations Conference*, Denver, CO, June 5-9, 2017, AIAA 2017-3785, pp. 1-14.

[4] G. Warwick. (2014, Jan. 27) NASA, Boeing Test Low-Drag Truss-Braced Wing Concept, High-Aspect-Ratio, Truss-Braced Wing Promises Marked Fuel Savings. *Aviation Week and Space Technology*, . 1.

[5] J. R. Chambers, *Innovation in Flight: Research of the NASA Langley Research Center on Revolutionary Advanced Concepts for Aeronautics*: NASA History Division, NASA SP-2005-4539, 2005.

[6] D. Montalvao, N. M. M. Maia, *et al.*, "A Review of Vibration-Based Structural Health Monitoring with Special Emphasis on Composite Materials," *Shock and vibration digest*, vol. 38, no. *4*, pp. 295-324, 2006.

[7] V. S. Papapetrou, A. Y. Tamijani, *et al.*, "Preliminary Wing Study of General Aviation Aircraft with Stitched Composite Panels," *Journal of Aircraft*, vol. 54, no. *2*, pp. 704-715, March - April 2016.

[8] M. Tamayama, K. Saitoh, *et al.*, "Effect of Vibration Data Preprocessing for Flutter Margin Prediction," in *Proc. 1st Int'l Symposium on Flutter and its Application*, Tokyo, Japan, May 15-17, 2017, pp. 97-104.

[9] E. Livne, "Aircraft Active Flutter Suppression State of the Art and Technology Maturation Needs," in *Proc. 58th AIAA/ASCE/AHS/ASC Structures, Structural Dynamics, and Materials Conference*, Grapevine, Texas, Jan. 9-13, 2017, AIAA 2017-1119, pp. 1-83.

[10] C. Briggs, "Design and Implementation of a Flutter Suppression Experiment," in *Proc. AIAA Atmospheric Flight Mechanics Conference*, Denver, CO, June 5-9, 2017, AIAA 2017-4357, pp. 1-17.

[11] S. Raja and A. Upadhya, "Active Control of Wing Flutter using Piezoactuated Surface," *Journal of aircraft*, vol. 44, no. *1*, pp. 71-80, January–February 2007.

[12] F. Kopsaftopoulos, R. Nardari, *et al.*, "A Stochastic Global Identification Framework for Aerospace Structures Operating under Varying Flight States," *Mechanical Systems and Signal Processing*, vol. 98, pp. 425-447, May 2018.

[13] J. Bakunowicz and P. Rzucidło, "Measurement and Analysis of Certain Flight Parameters Based on MEMS Sensors," *Journal of Sensors and Sensor Systems*, vol. 6, no. *1*, p. 211222, May 2017.

[14] C.-g. Pak, "Unsteady Aerodynamic Force Sensing from Strain Data," *AIAA Journal of Aircraft*, pp. 1-10, Feb. 9 2017.

[15] C.-g. Pak, "Wing Shape Sensing from Measured Strain," *AIAA Journal*, vol. 54, no. *3*, pp. 1064-1073, March 2016.

[16] S. Kota, P. Flick, *et al.*, "Flight Testing of the Flexfloil Adaptive Compliant Grailing Edge," in *Proc. 54th AIAA Aerospace Sciences Meeting*, San Diego, Ca, Jan. 4-8, 2016, AIAA 2016-0036, pp. 1-14.

[17] W. C. Wilson, J. P. Moore, *et al.*, "Surface Acoustic Wave Vibration Sensors for Measuring Aircraft Flutter," in *Proc. IEEE International Conference on Prognostics and Health Management (ICPHM)*, Ottawa, ON, Canada, June 20-22, 2016, pp. 1-7.

[18] C. Li, W. Chen, *et al.*, "A Noncontact FMCW Radar Sensor for Displacement Measurement in Structural Health Monitoring," *Sensors*, vol. 15, no. *4*, pp. 7412-7433, 2015.

[19] C. Gentile, "Application of Microwave Remote Sensing to Dynamic Testing of Stay-Cables," *Remote Sensing*, vol. 2, no. *1*, pp. 36-51, 2010.

[20] C. A. Leckey, M. D. Rogge, *et al.*, "Guided Waves in Anisotropic and Quasi-Isotropic Aerospace Composites: Three-Dimensional Simulation and Experiment," *Ultrasonics*, vol. 54, no. *1*, pp. 385-394, 2014.